BMC Genomics

RESEARCH Open Access

Large-scale integration of meta-QTL and genome-wide association study identifies genomic regions and candidate genes for photosynthetic efficiency traits in bread wheat

Ming Chen[1,2], Tao Chen[1,2], Letong Yun[1,2], Zhuo Che[1], Jingfu Ma[1,3], Binxue Kong[1,3], Jiangying Long[1,2], Chunhua Cheng[1,2], Kaiqi Guo[2], Peipei Zhang[1], Lijian Guo[1] and Delong Yang[1,2*]

Abstract

Background Improving photosynthetic efficiency is an essential strategy for advancing wheat breeding progress. Integrating wheat genetic resources provides an opportunity to discover pivotal genomic regions and candidate genes (CGs) for photosynthetic efficiency traits in wheat.

Results A large-scale meta-QTL (MQTL) analysis was performed with 1363 initial quantitative trait loci (QTLs) for photosynthetic efficiency traits extracted from 66 independent QTL mapping studies over the past decades. Consequently, 718 initial QTLs were refined into 74 MQTLs, which were distributed on all wheat chromosomes except 1D, 3 A, 4B, and 5B. Compared with the confidence interval (CI) of the initial QTL, the CI of the identified MQTL was 0.03 to 10.97 cM, with an average of 1.46 cM, which was 20.46 times narrower than that of the original QTL. The maximum explained phenotypic variance (PVE) of the MQTL ranged from 7.43 to 20.42, with an average of 11.97, which was 1.07 times higher than that of the original QTL. Of these, 54 MQTLs were validated using genome-wide association study (GWAS) data from different natural populations in previous research. A total of 3,102 CGs were identified within the MQTL intervals, where 342 CGs share homology with rice, and 1,043 CGs are highly expressed in leaves, spikes, and stems. These CGs were mainly involved in porphyrin metabolism, glyoxylate, dicarboxylate metabolism, carbon metabolism and photosynthesis antenna proteins metabolism pathways by the in silico transcriptome assessment. For the key CG *TaGGR-6A* (*TraesCS6A02G307700*) involved in the porphyrin metabolism pathway, a functional kompetitive allele-specific PCR (KASP) marker was developed at 2464 bp (A/G) position within the 3′ untranslated region, successfully distinguishing two haplotypes: *TaGGR-6A-Hap I* (type AA) and *TaGGR-6A-Hap II* (type GG). Varieties with the *TaGGR-6A-Hap II* allele exhibited approximately 13.42% and 11.45% higher flag leaf chlorophyll content than those carrying the *TaGGR-6A-Hap I* allele. The elite haplotype *TaGGR-6A-Hap II* was positively

*Correspondence:
Delong Yang
yangdl@gsau.edu.cn

Full list of author information is available at the end of the article

selected during wheat breeding, as evidenced by the geographical and annual frequency distributions of the two *TaGGR-6A* haplotypes.

Conclusion The findings will give further insights into the genetic determinants of photosynthetic efficiency traits and provide some reliable MQTLs and putative CGs for the genetic improvement of photosynthetic efficiency in wheat.

Keywords Wheat, Photosynthetic efficiency traits, Meta-analysis, Candidate genes, Haplotype analysis

Introduction

Wheat (*Triticum aestivum* L.) is one of important staple food crops worldwide, providing about 20% of the calories consumed in the global diet [1]. The increasing pace of global food crisis is staggering in the context of adverse global climate change, ever-growing world population and reduction in arable land [2, 3]. It is estimated that wheat production must increase by 60% to meet the food demand of the projected global population of 9.6 billion by 2050 [4]. To address these concerns, significant strides have been made on elite trait-based breeding to accelerate grain yield improvement.

Wheat yield is a complex trait influenced by various agronomic traits, where photosynthesis plays a critical role. Photosynthesis captures solar energy and represents the main driving force for plant growth, biomass accumulation and sink storage [5]. Optimizing photosynthesis represents a feasible strategy to increase cereal yield [6]. The efficiency of photosynthesis is a key indicator of photosynthetic capacity in plants [7–9]. Several important photosynthetic parameters, consisting of chlorophyll content, photosynthetic rate, stomatal conductance and so on, used to assess plant photosynthetic performance can significantly impact wheat growth, development, and final yield [10, 11]. The grain chlorophyll contents with high photosynthetic capacity and grain filling rate show significant positive correlation [12]. Elongating the duration of effective photosynthesis could increase the net photosynthetic rate and positively contributes to grain yield potential [13]. It is universally acknowledged that photosynthetic-related traits, including leaf morphology, leaf angle and stomatal morphology also have effect on wheat yield [14]. Optimal leaf shape and size are essential characteristics for efficient absorption of sunlight energy and its conversion into grain yield in wheat [15]. Gas exchange between plants and the environment is determined by stomatal conductance. The size and density of stomata are closely related to the efficiency of carbon dioxide and water transfer, which in turn influences the process of photosynthesis and overall photosynthetic efficiency [16]. In recent years, research on genetic improvement of photosynthetic efficiency in wheat has made remarkable progress. Through in-depth exploration of the molecular mechanism underlying photosynthesis, researchers have successfully identified several key genes associated with photosynthetic efficiency, and utilized gene editing technology to precisely modify these genes, thereby enhancing the photosynthetic efficiency and yield of wheat [17, 18]. Although the aforementioned genes have achieved remarkable results in the genetic improvement of wheat photosynthetic efficiency, the regulatory network of wheat photosynthetic efficiency is still complex and not fully elucidated. Therefore, it is important to continue to deepen the understanding of the genetic mechanism of photosynthetic efficiency traits in wheat and to identify more key genes.

In recent decades, quantitative trait locus (QTL) mapping associated with photosynthetic efficiency traits has been extensively discovered in different genetic backgrounds [10, 19–23]. However, the accuracy of QTL identification is affected by several factors, including the density of molecular markers, the complexity of the parental genetic backgrounds, and the statistical models used [24, 25]. To overcome these limitations, meta-QTL (MQTL) analysis which incorporates molecular markers and QTL detected from various genetic backgrounds and environments can identify reliable, stable and consistent MQTL regions and candidate genes (CGs) linked to traits in wheat [26]. The MQTL method can be directly applied to wheat genetic improvement without being influenced by genetic backgrounds, thereby enhancing breeding efficiency and accuracy [27, 28].

The combination of MQTL and genome-wide association studies (GWAS) is of great importance in genetics, and by overlaying GWAS results with MQTL data, we can more precisely identify genomic regions associated with photosynthetic efficiency. This improvement not only integrates raw QTL results from different genetic backgrounds but also improves the accuracy and reliability of QTL mapping, thus accelerating the identification of CGs [29]. This study provided a breakthrough solution to the challenge of genetic resolution of photosynthetic efficiency, a complex trait, through the systematic integration of MQTL and GWAS. Compared with previous studies, the data collected in this study are larger in scale and more extensive in trait coverage, demonstrating significant advantages in data size and trait resolution dimensions. The increasing and intensive application of MQTL has effectively revealed the complex genetic architecture of multigene quantitative traits in wheat

[30]. Among previous MQTL studies, three or more have focused explicitly on traits related to the photosynthetic rate, such as chlorophyll content and flag leaf size [31–33]. In the present study, the first large-scale integration of photosynthetic efficiency-related traits was conducted to provide a comprehensive systematic analysis of photosynthetic efficiency in wheat for a more thorough discovery of multiple MQTLs and CGs in wheat.

The objective of this study was to conduct an MQTL analysis related to wheat photosynthetic efficiency based on QTL mapping studies published over the past few decades and to identify key CGs in the important genomic intervals to pinpoint excellent haplotypes. This study will offer further insight into the genetic determinants for photosynthetic efficiency, and some valuable putative CGs will be suggested to be employed for the wheat improvement.

Results

Study on the characteristics of QTLs related to wheat photosynthetic efficiency

Between the years 2007 and 2024, a total of 66 independent QTL mapping studies related to photosynthetic efficiency traits were conducted, with the majority of these studies being published between 2014 and 2022. These studies involved 61 recombinant inbred line (RIL) populations and 15 doubled haploid (DH) populations (Fig. 1a-b, Table S1). As these lines of the permanent mapping populations were genetically stable and could be used for phenotyping the yield-related traits for years under different environment conditions. As a result, 1,363 QTLs for wheat photosynthetic efficiency were collected, including 588 QTLs for photosynthetic parameters and 775 QTLs for photosynthetic-related traits that influence photosynthetic parameters (Fig. 1c). These 1,363 reported QTLs distributed among all 21 wheat chromosomes, where 78.94% (1076/1363) were distributed on the A and B sub-genomes. Among them, chromosome 7A contained the highest number of QTLs with

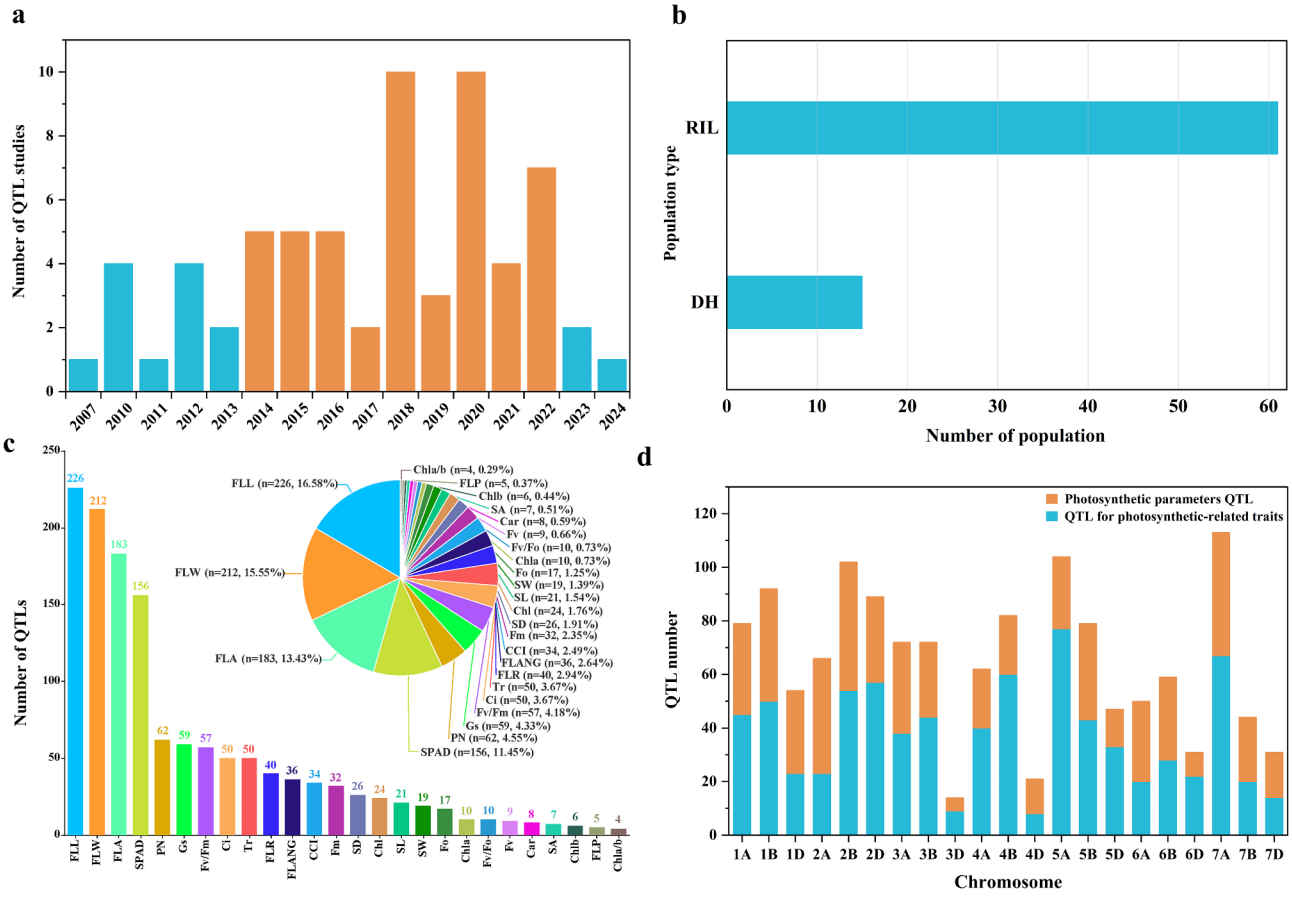

Fig. 1 The information of QTL for photosynthetic parameters and photosynthetic-related traits in previous QTL mapping studies used for meta-QTL analysis. (**a**) The time distribution of previous QTL mapping studies. The orange column shows a greater number of published studies, while the blue column indicates a lesser number of published studies. (**b**) The population type of pervious QTL mapping studies. (**c**) The proportion of QTL for photosynthetic parameters and photosynthetic-related traits. (**d**) The distribution of QTL on chromosomes

113, followed by chromosome 5A with 104 and chromosome 2B with 102, chromosome 3D harbored the lowest number of QTLs with only 14 (Fig. 1d). Correspondingly, the phenotypic variation explained (PVE) value of individual QTLs range from 0.01 to 72.72% with a mean value of 11.18%. Some QTL have high PVE values. These QTL with high PVE values may be statistical artifacts due to small population size, but they may also truly reflect some important biological effects. The 95% confidence intervals (CIs) ranged from 0.03 cM to 101.4 cM, with approximately 56% of the initial QTLs having a CI of less than 10 cM. The logarithm of the odds (LOD) values ranged from 2 to 48.64, with 59% of the initial QTLs having a LOD value that fell from 3 to 5.

Construction of consensus genetic map

The 76 individual genetic maps were integrated into the reference map to generate a consensus map (Table S2), containing 26,511 markers with an average of 1,559 markers per chromosome. The total length of the consensus map was 2,741.78 cM, with an average length of 161.28 cM per chromosome. The markers were unevenly distributed across the chromosomes while chromosome 1B harboring the highest number of markers with 3,544 (Fig. 2).

Identification of MQTLs related to wheat photosynthetic efficiency

Only 718 QTLs from 66 independent QTL studies were successfully projected onto the consensus map. Based on the criteria of the lowest model value and at least two overlapping initial QTLs, these initial QTLs were grouped into 74 MQTLs (Table 1; Table S3). Among the 74 identified MQTLs, all of them comprised at least two initial QTLs, with 97.29% (72/74) of MQTLs including three or more initial QTLs, and 66.22% (49/74) of MQTLs being made up of 11 to 50 initial QTLs while MQTL-7A.3 (61), MQTL-7A.4 (57) and MQTL-7A.5 (58) contained more than 50 initial QTLs (Fig. 3a). These MQTLs were distributed on 17 chromosomes except 1D, 3A, 4B, and 5B with an average of four MQTLs per chromosome (Fig. 3b). The average CI of MQTLs was 20.46 times smaller than that of initial QTLs with significant differences among different chromosomes. The CIs of chromosomes 3B and 1A decreased by 81.09 times and 58.83 times, respectively, followed by chromosomes 2B and 7A with reduction of 53.36 times and 33.93 times, respectively (Fig. 3c). The much smaller CIs demonstrate a significant improvement in the mapping accuracy of these MQTLs (Fig. 4).

All identified MQTLs were associated with at least two traits related to photosynthetic efficiency. Of the 74 MQTLs, 62 contain QTLs for flag leaf area (FLA), 27 contain three or more QTLs for FLA, and 58 and 57 MQTLs contain QTLs for flag leaf length (FLL) and the evolution

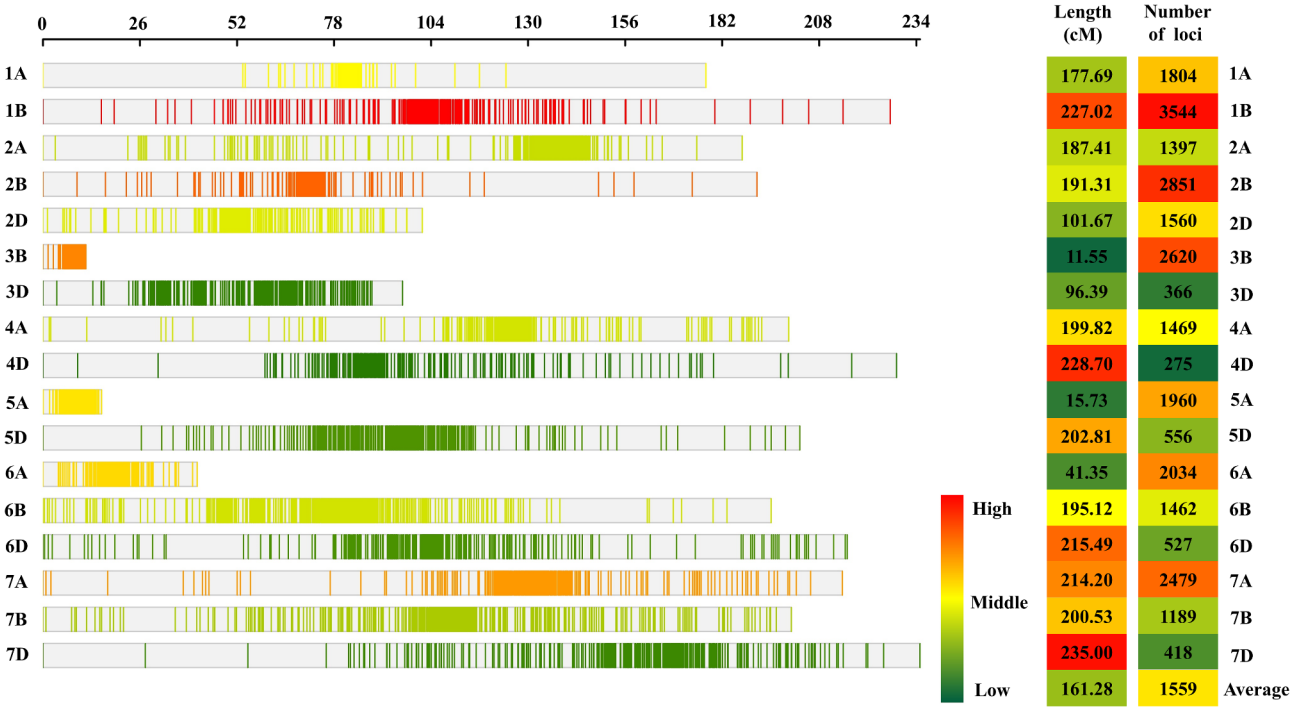

Fig. 2 Marker distribution on the consensus genetic map used for meta-QTL analysis. From red to green, the marker density in chromosome, the genetic length of chromosome, and the number of markers in chromosome decrease from high to low

Table 1 Summary of the 74 MQTLs detected in the present study (Continues)

MQTL ID	Position (cM)[b]	CI (cM)[c]	No. Of QTL	Traits[d]	Physical interval (Mb)	Flanking markers
MQTL-1 A.1[a]	79.72	0.06	20	FLW(4),FLL(4),FLA(3),SPAD(3),CCl(1),Others(5)	471.47-478.35	AX-110,567,101-AX-108,870,453
MQTL-1 A.2[a]	80.25	0.06	24	FLL(6),SPAD(4),FLW(4),FLA(3),Fm(2),Others(5)	533.44-535.02	wsnp_Ex_c6563_11378915-BS00110130_51
MQTL-1 A.3[a]	80.79	0.05	27	FLW(6),SPAD(4),FLL(4),Ci(2),Tr(2),Others(9)	532.24-544.36	wsnp_Ra_rep_c95460_83855592-BS00110877_51
MQTL-1 A.4	81.33	0.47	29	FLW(5),FLL(5),SPAD(4),FLA(3),Ci(2),Others(10)	542.43-577.84	Excalibur_c26688_138-RAC875_c53725_217
MQTL-1 A.5[a]	82.27	0.07	28	FLL(6),FLW(5),SPAD(4),FLA(4),Fm(2),Others(7)	582.86-589.47	RAC875_rep_c71278_345-BS00023419_51
MQTL-1B.1	99.6	0.09	30	FLL(4),SPAD(3),FLW(3),FLANG(3),Ci(2),Others(15)	303.68-478.72	BS00050630_51-BS00091871_51
MQTL-1B.2	100.86	0.6	32	FLL(4),Gs(3),PN(3),FLA(3),FLANG(3),Others(16)	536.70-638.93	RAC875_c102223_220-BS00089790_51
MQTL-1B.3[a]	102.88	0.15	18	FLA(2),FLL(2),SPAD(2),FLANG(2),FLR(2),Others(8)	646.67–664.30	Kukri_rep_c102001_420-Tdurum_contig55429_116
MQTL-1B.4	103.9	1.31	23	FLL(3),SPAD(2),FLANG(2),FLR(2),FLW(2),Others(12)	673.74-678.31	RAC875_c3001_1236-wsnp_Ex_c1058_2020681
MQTL-1B.5	113.36	1.11	15	Fm(3),SPAD(2),Fv/Fm(2),Fo(2),FLL(1),Others(5)	678.73-686.93	WMC367-TC88378
MQTL-2 A.1	131.57	1.76	13	SPAD(7),SD(1),Gs(1),PN(1),Ci(1),Others(2)	21.26–34.49	BS00021706_51-Ku_c23118_149
MQTL-2 A.2	134.22	2.34	17	SPAD(9),Gs(1),PN(1),Ci(1),Tr(1),Others(4)	34.66–51.49	BS00076693_51-BS00068196_51
MQTL-2 A.3[a]	137.06	0.12	24	SPAD(10),FLW(3),FLL(2),Gs(2),PN(2),Others(5)	62.30-68.25	BS00070693_51-GENE-1246_393
MQTL-2 A.4[a]	137.41	0.25	29	SPAD(9),FLL(3),FLA(3),Gs(3),PN(3),Others(8)	70.98–79.75	Jagger_c2047_362-BS00079443_51
MQTL-2 A.5	138.05	0.74	32	SPAD(9),PN(5),Gs(4),FLA(3),Ci(3),Others(8)	675.89-696.85	RAC875_rep_c113120_326-Ex_c23042_1024
MQTL-2 A.6[a]	138.68	0.06	28	SPAD(8),PN(4),Gs(3),Ci(3),FLW(3),Others(7)	709.04-712.72	wsnp_Ku_c54793_58953037-Ku_c13700_1189
MQTL-2 A.7	139.39	0.86	26	SPAD(8),PN(4),Gs(3),Ci(3),FLW(2),Others(6)	728.75-770.01	wsnp_Ex_c14953_23104041-Ra_c1757_256
MQTL-2B.1[a]	70.39	0.23	42	FLW(7),Gs(5),SPAD(5),FLL(4),Fv/Fm(4),Others(17)	10.78–14.04	BS00064570_51-Excalibur_c25445_1061
MQTL-2B.2	70.93	0.12	42	FLL(5),Gs(5),SPAD(5),FLW(5),PN(4),Others(18)	24.51–58.32	BS00070900_51-Tdurum_contig54704_176
MQTL-2B.3	71.81	0.12	43	FLW(8),SPAD(6),PN(4),Gs(4),FLANG(3),Others(18)	115.38-181.61	wsnp_BM140364B_Ta_2_3-TA001322-1176
MQTL-2B.4	72.21	0.61	42	SPAD(7),FLW(6),Gs(5),PN(4),FLANG(3),Others(17)	182.01-240.22	Kukri_c10054_567-WMC223
MQTL-2D.1	52.44	1.94	20	FLW(4),FLANG(2),FLA(2),FLL(2),Gs(2),Others(8)	6.63–20.76	RAC875_c12533_2006-JD_c63957_1176
MQTL-2D.2	61.96	1.79	6	FLL(2),FLA(2),FLW(1),FLR(1)	26.61–27.77	BS00009575_51-D_GB5Y7FA-02HINSP_259
MQTL-3B.1	8.26	0.08	17	FLW(4),FLA(3),PN(3),SPAD(2),FLL(2),Others(3)	479.87–587.00	BS00023645_51-Excalibur_c26662_218
MQTL-3B.2	8.82	0.1	17	FLW(5),FLA(3),PN(3),SPAD(2),FLL(1),Others(3)	669.71-779.13	wsnp_Ex_c3257_6003626-BS00024883_51
MQTL-3D.1	67.91	1.44	4	SD(2),Fv/Fm(1),SW(1)	129.02–297.50	Xwmc533-Xbarc1119
MQTL-3D.2	82.43	10.03	2	SD(1),Fv/Fo(1)	462.53–564.60	Xwmc492-Xcfd223
MQTL-4 A.1[a]	114.46	0.42	7	FLL(4),FLA(2),FLW(1)	4.47–11.81	Xcfa2173-BS00022177_51
MQTL-4 A.2	119.85	1.89	14	FLA(7),FLL(6),FLW(1)	12.20-16.19	BS00065863_51-wsnp_Ex_c28429_37553452
MQTL-4 A.3	125.22	0.1	21	FLL(7),FLA(6),PN(2),SW(1),Fv/Fm(1),Others(4)	515.84–576.70	Xwmc89-wsnp_Ex_c23248_32488191
MQTL-4 A.4	125.79	0.06	21	FLL(7),FLA(6),PN(2),SW(1),Fv/Fm(1),Others(4)	591.70-617.09	wsnp_Ex_c21383_30513824-BS00022418_51
MQTL-4 A.5	126.58	0.22	20	FLL(6),FLA(6),PN(2),Tr(2),SW(1),Others(3)	636.97-735.74	BS00062059_51-wPt-1007
MQTL-4 A.6	126.77	0.11	20	FLL(7),FLA(5),PN(2),Tr(2),SW(1),Others(3)	660.79-727.11	BobWhite_c43728_100-RFL_Contig2531_987
MQTL-4D.1	80.32	4.58	3	FLW(1),PN(1),Tr(1)	238.37-274.22	Xcfd193-GENE-2128_156

Table 1 (continued)

MQTL ID	Position (cM)[b]	CI (cM)[c]	No. Of QTL	Traits[d]	Physical interval (Mb)	Flanking markers
MQTL-4D.2	98.68	10.97	4	Fm(1),Fv/Fm(1),SPAD(1),Fo(1)	439.66-461.51	Xcfd89-Xbcd15
MQTL-4D.3	109.55	4.59	5	Fm(1),Fv/Fm(1),SPAD(1),Fo(1),FLW(1)	477.12-484.65	Xfbb178-Xwmc399
MQTL-5 A.1	6.24	0.78	32	FLA(9),FLL(8),FLANG(6),FLR(2),SPAD(2),Others(5)	37.06–70.73	Excalibur_rep_c108066_112-Xbarc56
MQTL-5 A.2	7.79	0.28	35	FLL(11),FLA(8),FLANG(6),FLR(2),FLW(2),Others(6)	437.20-585.40	BobWhite_c17440_130-wsnp_Ex_c31799_40545376
MQTL-5 A.3	9.66	0.03	38	FLL(9),FLA(9),FLANG(6),SPAD(4),FLW(3),Others(7)	588.84-647.36	Kukri_c64923_717-Tdurum_contig15047_186
MQTL-5D.1	65.92	2.24	4	FLL(3),Chl(1)	41.81–44.61	AX-89,752,452-AX-110,024,138
MQTL-5D.2	71.55	0.65	4	SL(1),FLA(1),FLL(1),Chl(1)	229.36-290.67	Xgdm68-AX-111,117,089
MQTL-7 A.5	133.02	0.22	58	FLW(12),FLANG(8),FLL(7),FLA(7),SPAD(4),Others(20)	115.81-343.84	BS00038787_51-wsnp_Ra_c23253_32762188
MQTL-7B.1	94.93	5	4	FLA(2),FLL(1),Fv/Fm(1)	553.18-723.21	AX-109,902,366-Xbarc1073
MQTL-7B.2	103.99	0.24	9	Tr(2),Ci(2),SPAD(2),Chla/b(1),FLL(1),Others(1)	670.84-708.47	wPt-3533-Tdurum_contig44876_1362
MQTL-7B.3	105.54	1.85	10	SPAD(3),Tr(2),Ci(2),CCI(1),FLL(1),Others(1)	625.88-730.15	BobWhite_c12256_96-Excalibur_rep_c69840_85
MQTL-7B.4	107.51	0.41	19	Tr(4),Ci(3),SPAD(2),PN(2),Gs(2),Others(6)	645.12-744.11	wsnp_Ku_c16295_25148628-RAC875_c42674_239
MQTL-7B.5	109.3	0.75	18	FLW(3),FLL(3),FLA(3),Ci(2),SPAD(2),Others(5)	657.87-732.39	wsnp_BE605194B_Ta_2_7-Xbarc182
MQTL-7B.6	112.73	0.94	14	Ci(3),SPAD(2),Tr(2),Gs(1),PN(1),Others(5)	726.13-747.19	BobWhite_rep_c50003_377-wPt-2878
MQTL-7D.1	127.47	2.64	3	SPAD(1),Fv/Fo(1),Chla(1)	30.83–58.25	Xbcd588-Xgwm130
MQTL-7D.2	151.04	2.88	13	FLW(3),FLL(2),Chla(1),Fo(1),Fv(1),Others(5)	52.94-102.54	Xbarc92-IAAV2530
MQTL-7D.3	168.13	1.61	11	FLW(6),FLL(3),FLA(1),Chl(1)	211.40-364.63	wsnp_CAP11_c2839_1425826-Xwmc221
MQTL-7D.4	170.71	2.37	11	FLW(5),FLL(2),FLA(1),Chl(1),Ci(1),Others(1)	414.28-531.58	Xwmc630-Xbarc121
MQTL-7D.5	173.78	2.56	7	FLW(4),Gs(1),SPAD(1),FLL(1)	530.67-587.91	wsnp_BE497845D_Ta_1_1-Xbarc111

[a]Core MQTL

[b]The most likely position on consensus map

[c]The confidence interval (95%) of MQTL on consensus map

[d]FLW: flag leaf width; FLA: flag leaf area; FLANG: flag leaf angle; SPAD: the evolution of soil plant analysis development; Fo: initial fluorescence; Fv: variable fluorescence; CCI: chlorophyll index; Gs: stomatal conductance; CI: confidence interval; Fv/Fo: maximum primary yield of PSII photochemistry; Chl: chlorophyll content; Tr: transpiration rate

Each MQTL only lists the trait types of the top five QTL

of soil plant analysis development (SPAD), respectively. Among them, 55 MQTLs simultaneously contain QTLs for both FLA and FLL, 51 for both FLA and SPAD, 44 for both FLL and SPAD, and 43 MQTLs contain QTLs for all three traits: FLA, FLL, and SPAD. In addition to the major traits mentioned above, some MQTLs also broadly encompassed multiple traits related to photosynthetic efficiency. For example, MQTL-7A.5 was simultaneously associated with 16 photosynthetic efficiency-related traits: net photosynthetic rate (Pn), stomatal conductance (Gs), flag leaf angle (FLANG), maximum photosynthetic efficiency of optical system II (Fv/Fm), intercellular CO_2 concentration (Ci), flag leaf width (FLW), stomatal length (SL), chlorophyll a/chlorophyll b (Chla/b), chlorophyll a (Chla), chlorophyll index (CCI), stomatal density (SD), transpiration rate (Tr), maximum fluorescence (Fm), FLA, FLL, and SPAD (Table 1; Table S3).

Validating MQTLs using MTA identified in previous GWAS studies

The physical positions of the MQTLs identified in this study and the marker trait associations (MTAs) from 18 previous GWAS studies were used for comparison to further determine the reliability of MQTL for photosynthetic efficiency. Accordingly, 72.97% (54/74) of the identified MQTLs were co-located with 758 MTAs peak positions early reported in GWAS for photosynthetic efficiency in wheat (Table S4). Among these MQTLs, 37 were identified in at least two studies. MQTL-5A.2 was identified in nine GWAS studies, making it the most frequently observed, followed by MQTL-2B.2 and

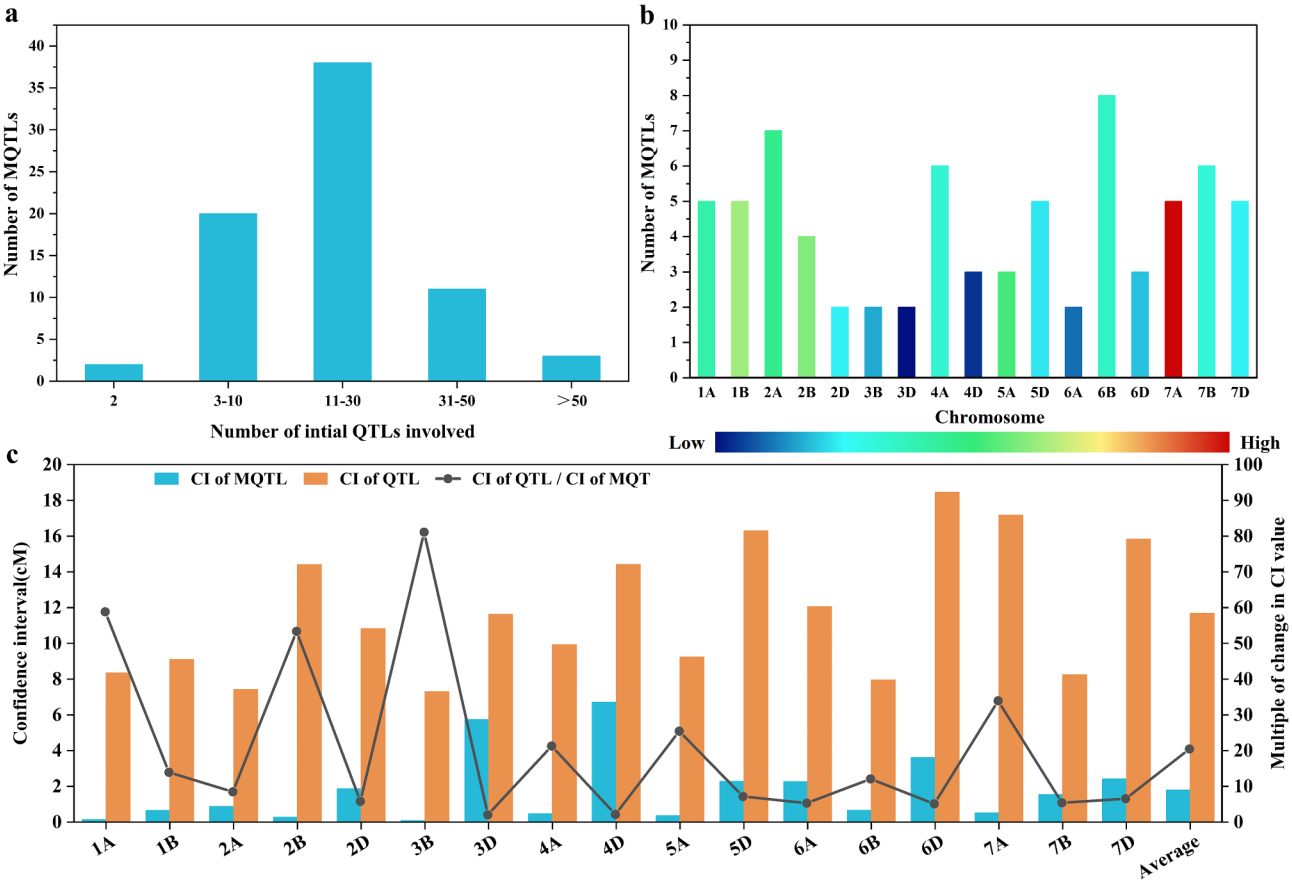

Fig. 3 Basic information of MQTL obtained in meta-QTL analysis. (**a**) The number of MQTL harboring different numbers of QTL. (**b**) The number of MQTL and average number of initial QTL projected on a single MQTL in different chromosomes. From blue to red, the number of QTL contained in MQTL increases from low to high. (**c**) The reduction degree of QTL confidence interval (CI, 95%) after meta-QTL analysis. The orange and blue bars represent the average CI length (cM) of MQTL and initial QTL on chromosomes, respectively, and the broken line represents the reduction folds of the QTL CI length

MQTL-7B.1 each identified in seven studies, MQTL-6B.3 and MQTL-6B.7 coexisted with the largest number of 153 and 210 MTAs, respectively (Fig. 5).

Identification and functional analysis of CGs within MQTL regions

An in-depth exploration was conducted to uncover important CGs via integrating homology alignment with sequence information from plant genome databases. In this study, based on the detailed seanning for known rice genes resulted in the obtainment of 530 functional CGs affecting rice photosynthetic efficiency (Table S5). Using BLASTP analysis, 1,307 wheat orthologs of rice genes for photosynthetic efficiency were identified across wheat genomes. Only 342 genes were found within 74 MQTL intervals, with an average of 4 genes per MQTL (Table S6). Furthermore, by searching for the peak positions of MQTLs within a 2 Mb genomic range, 2,797 potential CGs were identified (Table S7). In summary, 3,102 potential CGs were identified through the two aforementioned methods. The expression analysis performed on CGs revealed that 1,043 key CGs with ≥ 2 transcripts per million (TPM) and highly expression in leaves, spikes, and stems at different developmental stages were selected for further in silico analysis (Table S8). Gene ontology (GO) enrichment and Kyoto Encyclopedia of Genes and Genomes (KEGG) pathway analysis were conducted with 1,043 CGs. The GO analysis indicated that the cellular process (472 CGs) and metabolic process (417 CGs) were the most relevant enriched terms related to biological processes. As for molecular functions, the most enriched GO terms were related to binding (461 CGs) and catalytic activity (391 CGs). In terms of cellular components, cellular anatomical entity (458 CGs) had the highest enrichment level (Fig. 6). The KEGG enrichment analysis showed that these putative genes were highly involved in the porphyrin metabolism (16 CGs), glyoxylate and dicarboxylate metabolism (16 CGs), carbon metabolism (32 CGs), and photosynthesis - antenna proteins (8 CGs) (Fig. 7). Notably, 186 CGs recurring in the top 20 of KEGG enrichment pathways were to perform expression analysis. In order to more intuitively demonstrate the expression characteristics of these CG genes, a heatmap was further drawn for visualization and analysis (Fig. 8).

Fig. 4 The chromosome distribution of the 74 discovered meta-quantitative trait loci (MQTLs). The circles from inside to outside represent the genetic map, original quantitative trait loci (QTL) numbers, confidence interval, R^2 values, physical position of MQTLs, and physical map (Mb), respectively

These 186 CGs could be divided into three classes. In class I, the genes were ubiquitously expressed in different tissues with varying degree of expression while in class II, the genes showed high expression in leaf and stem at the mid-flowering stage and finally in class III, the genes showed high expression in the spike and stem at the booting stage and early jointing stage. The high expression of class II genes during mid-flowering period and in leaves implies that they may be more closely related to photosynthetic efficiency. The key gene *TraesCS6A02G307700* (*TaGGR-6A*) belongs to class II genes, which involved in the porphyrin metabolism pathway for chlorophyll synthesis while its homologous gene in rice *LYL1* as a light-responsive gene showing highly expressed in the leaf. Furthermore, *TaGGR-6A* is highly expressed in the leaf across three different stages: One-leaf stage, Early tiller stage, and 2 days after flowering, with TPM values exceeding 200. Therefore, we selected *TaGGR-6A* for further investigation.

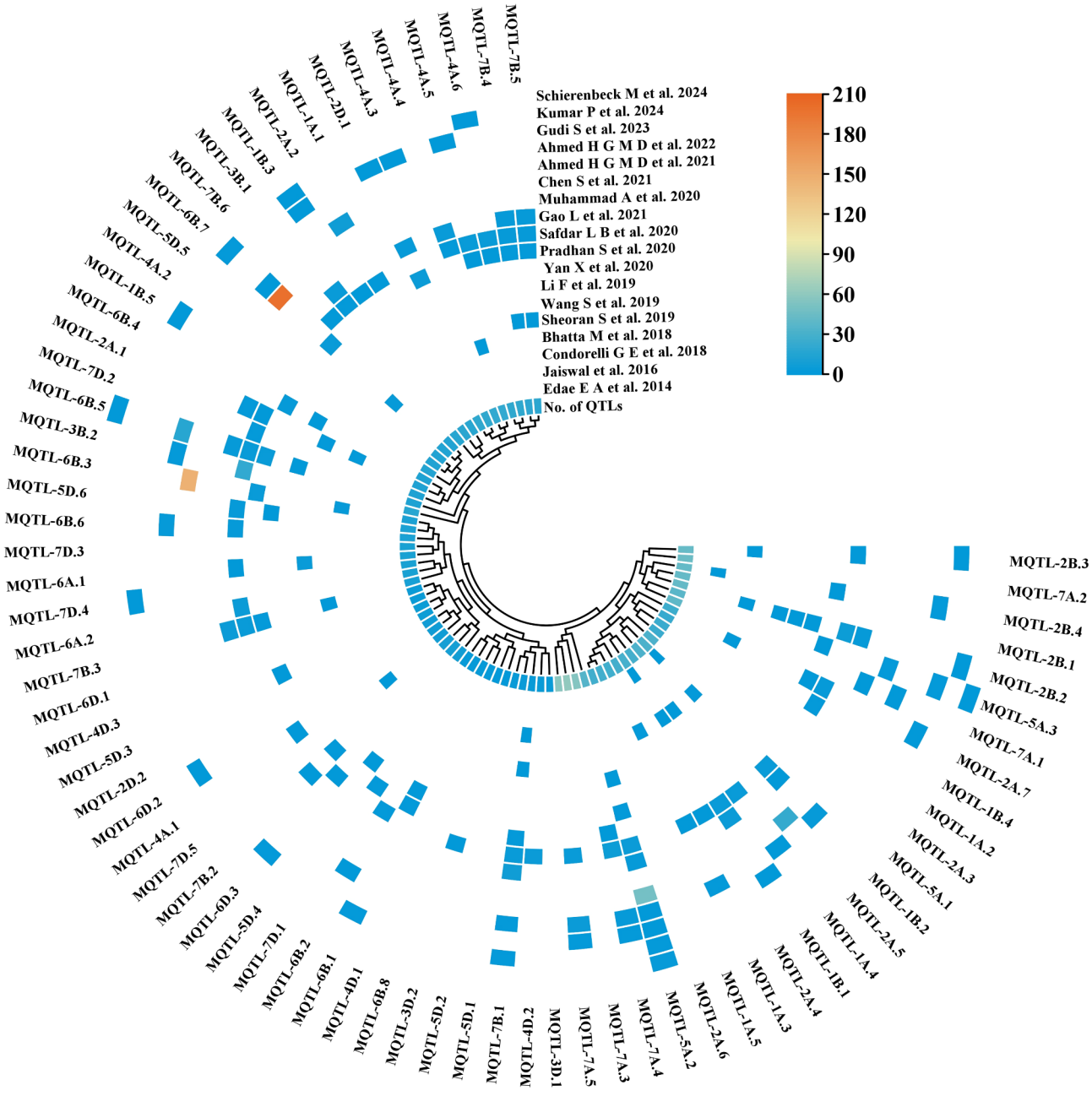

Fig. 5 Validation of meta-quantitative trait loci (MQTLs) by marker-trait associations (MTAs) in photosynthetic efficiency of wheat from genome-wide association study (GWAS) with different natural populations. The number of MTAs located in MQTL is increasing from blue to orange

Association analysis between *TaGGR-6A* gene haplotypes and chlorophyll content in wheat flag leaves

The polymorphic single nucleotide polymorphism (SNP) loci of the *TaGGR-6A* in wheat were identified by analyzing the variants in the genome sequence data of 1769 wheat varieties obtained from the Wheat Consortium website (http://wheat.cau.edu.cn/WheatUnion/, Accessed June 2024) (Table S9). Ten polymorphic SNP sites were identified in the key CG *TaGGR-6A* (Fig. 9a), seven in the promoter region, one within an exon, and two in the 3'UTR region. Owing to these variant sites, two haplotypes of *TaGGR-6A* were formed and designated *TaGGR-6A-hap I* and *TaGGR-6A-hap II*. A kompetitive allele-specific PCR (KASP) marker was developed based on a SNP at 2464 bp (A/G) to differentiate wheat germplasm associated with the two haplotypes.

Bioinformatics analysis indicated that the two SNPs at the *TaGGR-6A* promoter were involved in the formation of several transcription factor binding sites, including ARE and MYB (Fig. 9a). The genotyping was performed

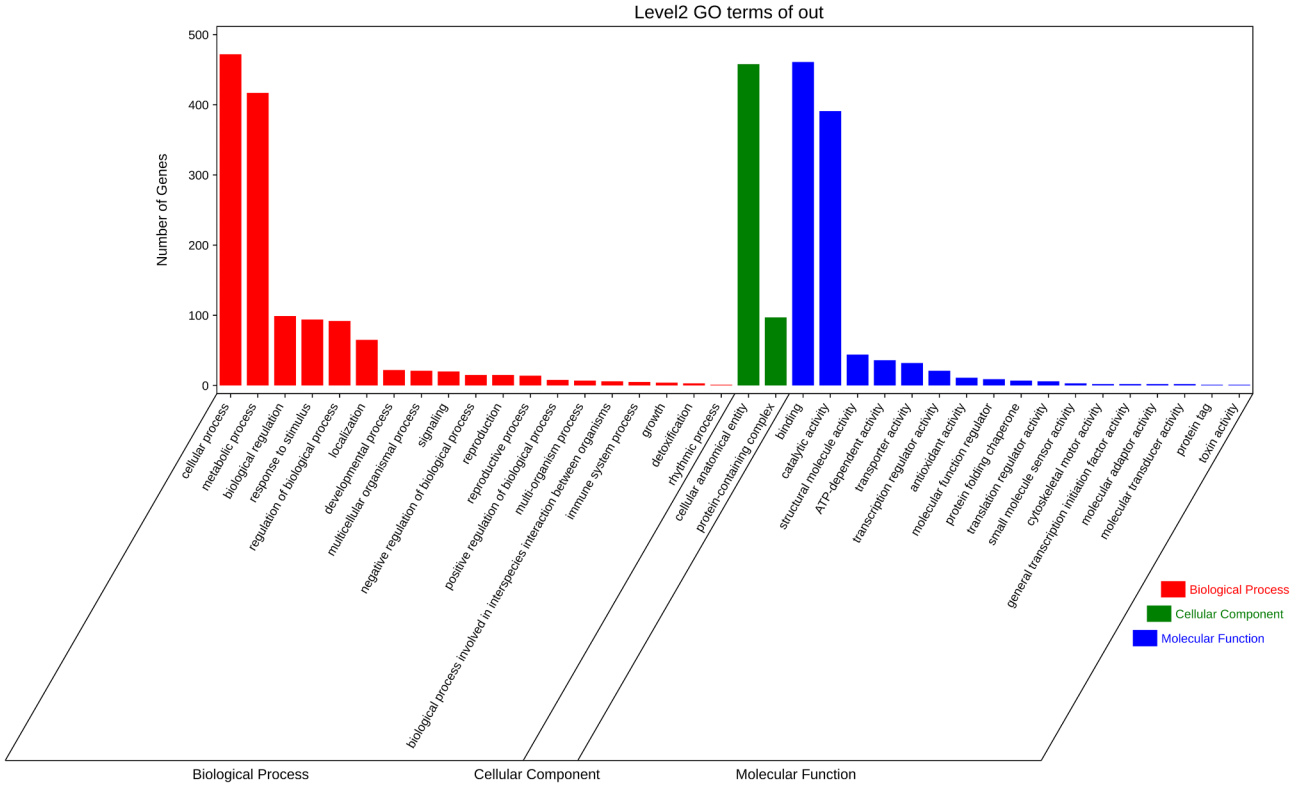

Fig. 6 Gene ontology (GO) terms for 1,043 putative candidate genes (CGs) from meta-quantitative trait locus (MQTL) regions

on 252 wheat accessions using the KASP marker (Table S10, Fig. 9b). The unique transcription factor binding sites MYB and ARE contained in the *TaGGR-6A-Hap II* promoter sequence may account for its superiority. To further explore the impact of the *TaGGR-6A* marker on chlorophyll content in wheat, the association analysis of the chlorophyll content in flag leaves was conducted on 252 wheat accessions with two different genotypes. The results showed that the wheat accessions with *TaGGR-6A-hap II* exhibited significantly higher chlorophyll content ($P < 0.05$) compared to those of *TaGGR-6A-hap II* in two different environments (Fig. 9c, Table S11). Therefore, the *TaGGR-6A-Hap II* haplotype may be an elite haplotype for improving flag leaf chlorophyll content.

Selection of *TaGGR-6A* haplotypes in wheat breeding

The wheat breeding process enabled the gradual accumulation of excellent haplotypes through steps such as parent selection, hybridization, descendant selection and evaluation, stabilization and purification of superior haplotypes. The geographic distribution of the two alleles of *TaGGR-6A* using 242 wheat accessions indicated that the haplotype *TaGGR-6A-hap II* with high SPAD were predominant in major wheat-growing regions of China, including Hebei (77%), Henan (72%), Shanxi (72%), Shandong (57%), and Shaanxi (56%) (Table S12, Fig. 10a). To further determine whether *TaGGR-6A-Hap II* has been positively selected during the course of wheat breeding in China, the frequency of the *TaGGR-6A* haplotype in 117 historical wheat populations was examined at decade intervals (Table S13). The results showed that the frequency of *TaGGR-6A-Hap II* was not as high as that of *TaGGR-6A-Hap I* before 2000, while the frequency of *TaGGR-6A-Hap II* increased from the pre-1981 (33%) to the post-2010 (71%) with a continuous increase (Fig. 10b). The results suggested that the *TaGGR-6A-Hap II* gene has been positively selected during wheat breeding to optimize wheat photosynthetic characteristics.

Discussion

Characteristics of QTL and MQTL related to wheat photosynthetic efficiency

Over the past few decades, numerous QTLs associated with wheat photosynthetic efficiency traits have created favorable conditions for elucidating the genetic basis of wheat photosynthetic efficiency. In this study, 588 QTLs related to photosynthesis parameters and 775 QTLs affecting photosynthesis-related traits from 66 independent QTL mapping studies were integrated with GWAS data for MQTL analysis; subsequently, CGs were screened using transcriptome data (Fig.).

Compared with previous studies on photosynthetic efficiency [31–33], the MQTL analysis demonstrated significant advantages. In terms of coverage and number

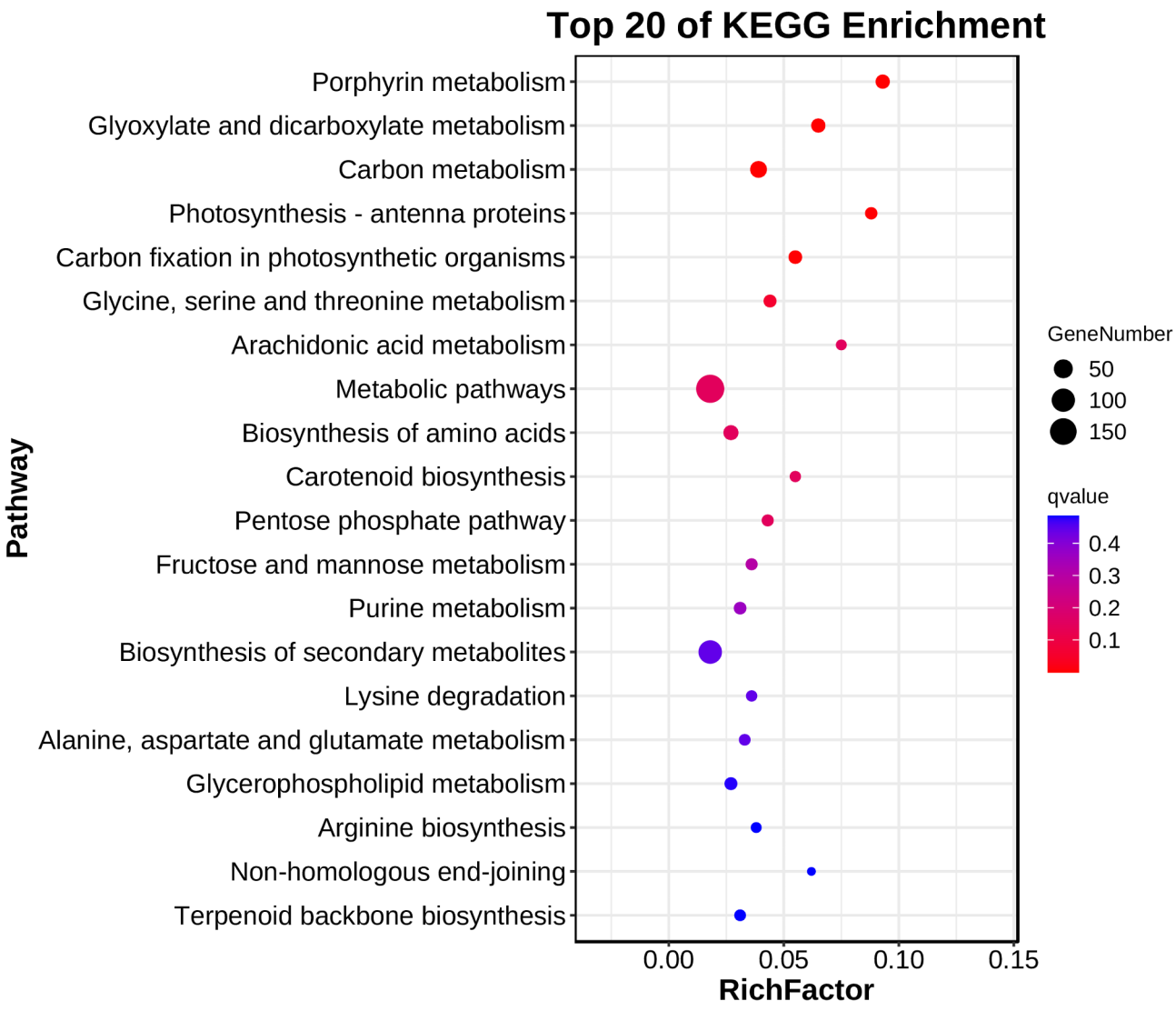

Fig. 7 Top 20 Kyoto Encyclopedia of Genes and Genomes (KEGG) enrichment pathways for 1,043 putative candidate genes (CGs) from meta-quantitative trait locus (MQTL) regions

of QTLs, a larger number of initial QTLs were utilized, ensuring the comprehensiveness and accuracy of genetic locus localization. In our study, the 718 initial QTLs were unevenly distributed onto 21 wheat chromosomes. This uneven distribution may be the result of a combination of various factors such as gene density, gene interactions, selection pressure, and genetic linkage. Most of the QTLs were concentrated in subgenomes A and B (about 78.94%). This finding aligns with previous research [32], validating the reliability of the mapping method.

The advantage of MQTL analysis lies in its ability to exclude the interference of factors such as genetic background, population type, and cultivation environment on QTLs, effectively integrating QTL data from different backgrounds [26]. In this study, this advantage was fully leveraged by increasing the number of initial QTLs, significantly enhancing the accuracy of MQTL analysis results [34]. Specifically, 718 initial QTLs were successfully mapped onto the consensus map and further refined into 74 MQTLs. Notably, 70.27% of the MQTLs were composed of more than 11 initial QTLs, and three MQTLs were based on over 50 initial QTLs, a proportion significantly higher than that in previous studies [31–33]. Furthermore, a detailed comparison of the MQTL analysis results with those of previous studies based on physical positions revealed that 55 out of the 74 MQTLs were co-located with previous findings [31–33]. This high degree of consistency not only validates the accuracy of the MQTL analysis but also further highlights the reliability of the QTL localization and analysis. Our study also revealed extensive overlap between direct phenotypic traits and derived traits for photosynthetic efficiency in MQTL. This finding highlights the complexity of the genetic architecture underlying photosynthetic efficiency,

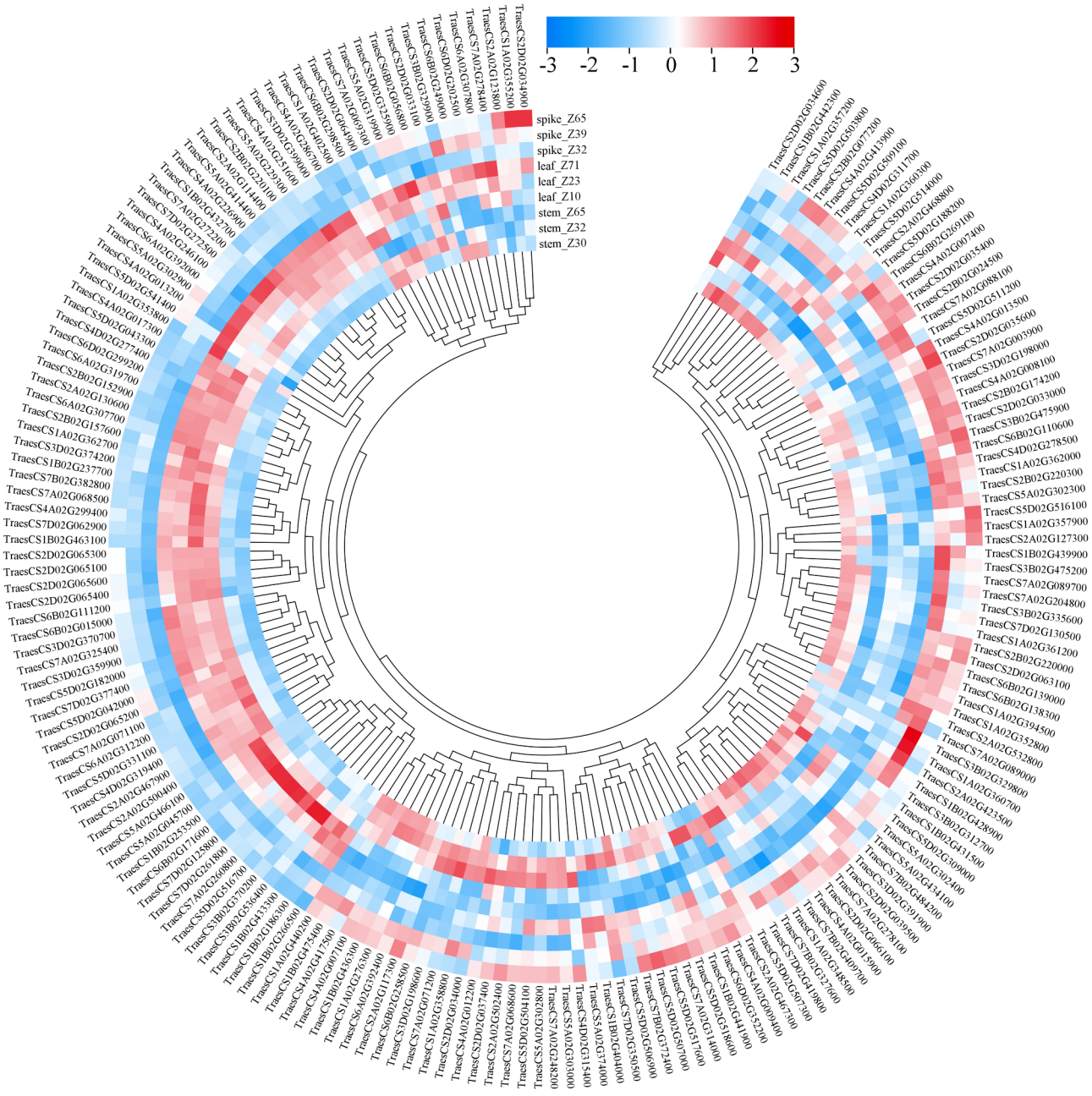

Fig. 8 Expression patterns of 186 candidate genes in different tissues at different stages. From blue to red, the expression value goes from low to high. Z10: One-leaf stage; Z23: Early tiller stage; Z30: Booting stage; Z32: Early jointing stage; Z39: Late jointing stage; Z65: Mid-flowering stage; Z71: 2 d after flowering

indicating that multiple traits interact in a coordinated way to optimize photosynthetic performance. Further investigating the connections between these MQTL and traits associated with photosynthetic efficiency will be helpful in developing wheat varieties that exhibit higher photosynthetic efficiency and increased yield.

MQTL analysis can integrate QTL information from different genetic backgrounds, thereby effectively reducing the CI of QTLs and improving the accuracy of CG prediction. Compared with the initial QTLs, the average CI of MQTLs was reduced by approximately 20.46 times, a significant reduction compared to previous study results [31–33], providing strong support for more accurate CG prediction and localization. Wheat photosynthetic efficiency is controlled by multiple genes and is easily influenced by environmental conditions. Identifying genomic regions closely related to and stable for photosynthetic efficiency is a prerequisite for utilizing molecular marker-assisted crop breeding. Based on the selection criterion, 15 MQTLs were selected in this

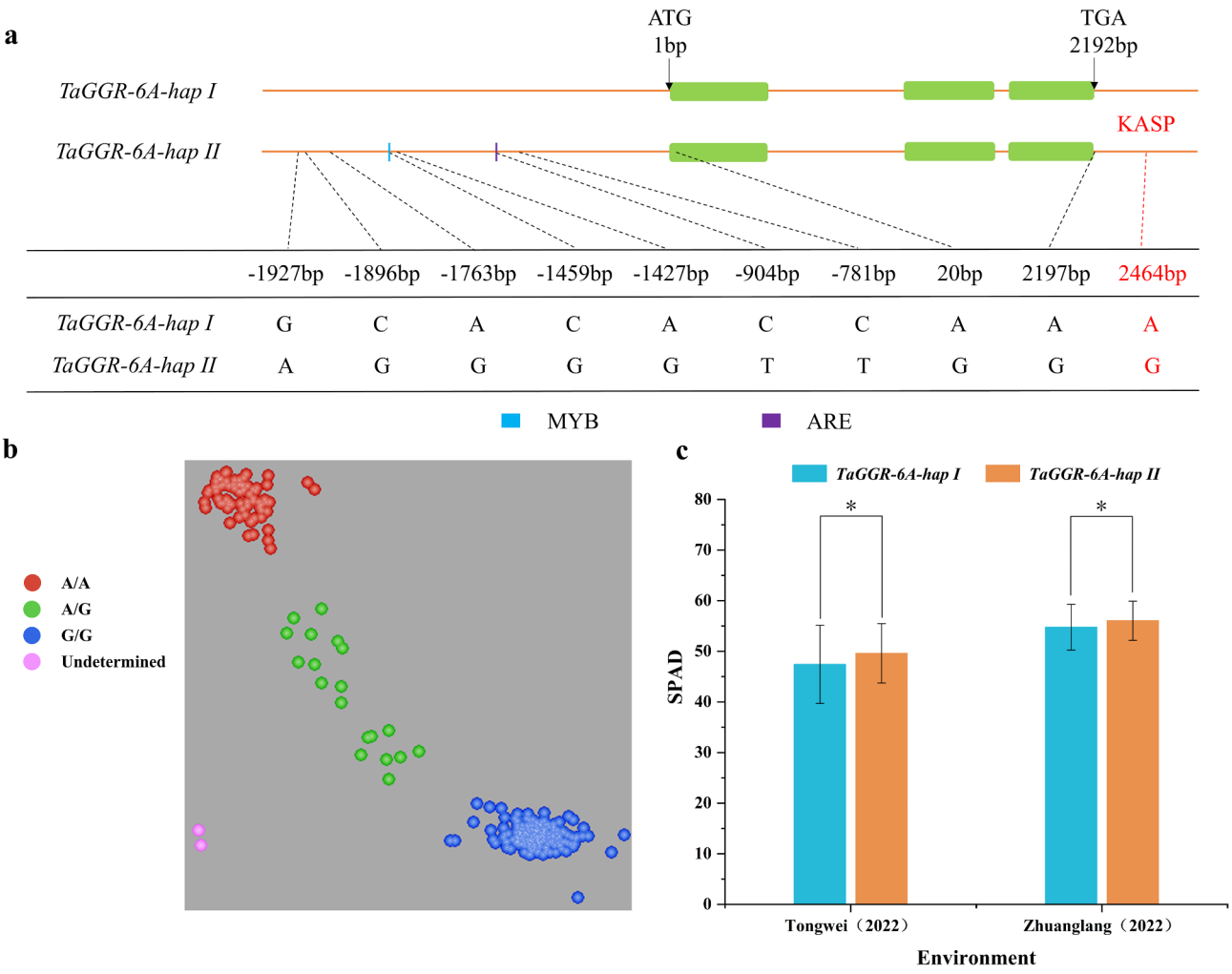

Fig. 9 Analysis of *TaGGR-6A* gene structure, genotyping and association with SPAD. (**a**) Schematic *TaGGR-6A* gene structure and main cis-element distribution of promoter. (**b**) kompetitive allele-specific PCR (KASP) genotyping scatter cluster diagram of *TaGGR-6A*. (**c**) Association analysis of *TaGGR-6A* allelic variation and SPAD in different environments

study as the primary CG search intervals (Table 1). The genetic intervals of these MQTLs are less than 1 cM, and the physical intervals are less than 20 Mb, with an average PVE and number of initial QTLs of 11.17% and 27, respectively. These core MQTLs lay a solid foundation for exploring their application in enhancing wheat photosynthetic efficiency.

CGs in MQTL and their roles in influencing photosynthetic efficiency

This study further confirmed that approximately 72.97% of the MQTLs matched the MTAs in GWAS. These results suggested that the influence of these genomic regions on photosynthetic efficiency traits may be less restricted by genetic background. On the other hand, the lack of correspondence with MTAs in GWAS may be attributed to genotype-environment interactions and variations in trait measurement, which could explain the discrepancy. These matching MQTLs and MTAs obtained through GWAS studies provide a foundation for effectively identifying CGs that regulate wheat photosynthetic efficiency.

Based on functional annotations and expression characteristics, 1043 key CGs showing high expression (TPM ≥ 2) at different developmental stages in leaves, spikes, and stems were selected for further analysis. The GO and KEGG analysis indicated that the most enriched metabolic pathways include porphyrin metabolism, glyoxylate and dicarboxylate metabolism, carbon metabolism, photosynthesis-antenna proteins, etc. Porphyrin metabolism, the cornerstone of chlorophyll synthesis, is essential for plants to effectively absorb and convert light energy [35]. Its proper functioning has a direct and critical impact on photosynthetic efficiency. Meanwhile, the smoothness of carbon metabolism and the photosynthetic carbon fixation pathway directly relate to plants'

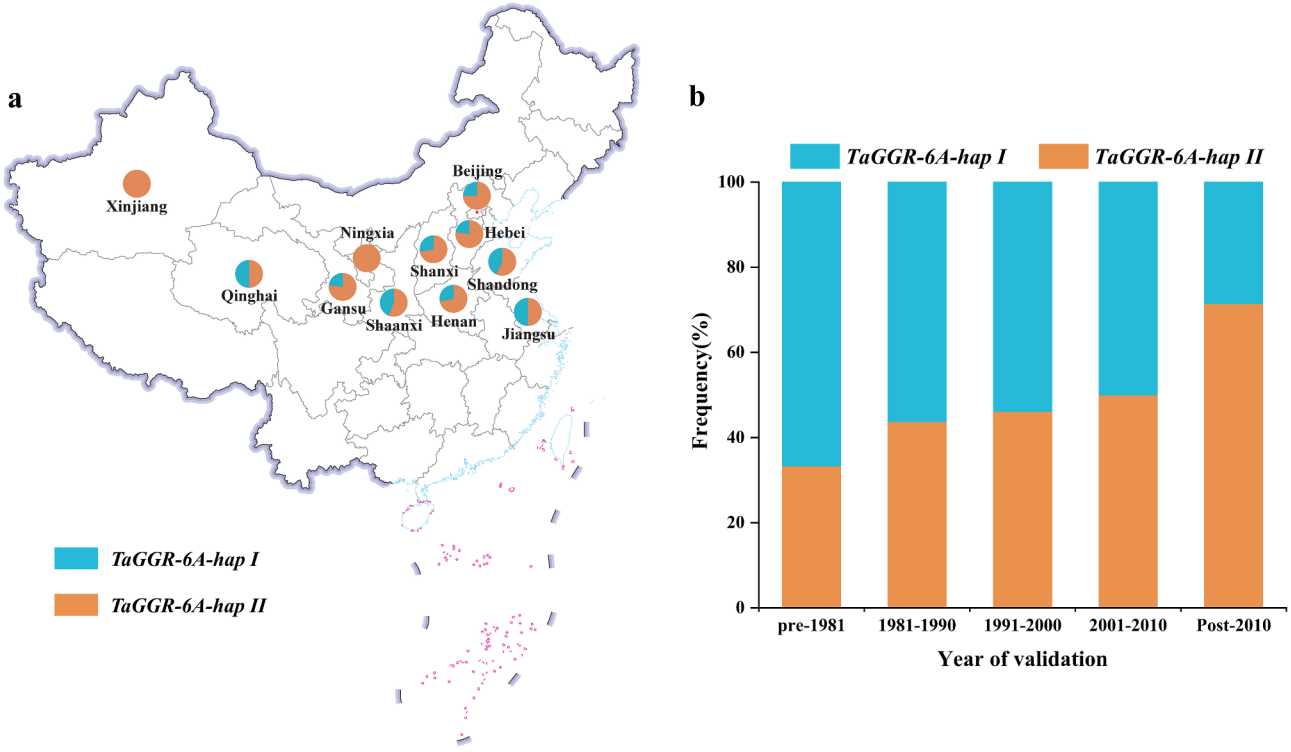

Fig. 10 Selection of *TaGGR-6A* haplotypes in wheat breeding in China. (**a**) Geographic distribution of varieties with *TaGGR-6A* haplotypes in China. (**b**) Variation of the proportion of haplotypes of *TaGGR-6A* with breeding age

efficiency in utilizing carbon dioxide and their ability to synthesize organic compounds, serving as essential drivers for enhancing photosynthetic efficiency [36]. Furthermore, the photosynthesis-antenna protein pathway plays an irreplaceable role in light energy capture and transfer, and its functional integrity is vital for maintaining efficient photosynthesis [37].

This study identified a CG, *TaGGR-6A*, associated with porphyrin metabolism within the MQTL interval. This gene affects the catalysis of geranylgeranyl diphosphate reduction to phytyl diphosphate, providing phytol for tocopherol and chlorophyll synthesis, and plays a crucial role in chlorophyll synthesis. Previous studies have shown that chlorophyll, composed of a porphyrin head group which contains magnesium, and of phytol, a prenyl side chain bound in ester linkage, is the most critical photosynthetic pigment in plants [35]. By searching for SNP variation sites within the *TaGGR-6A* gene in the Wheat Variation Database, corresponding KASP markers were developed to distinguish between the two haplotypes of *TaGGR-6A*. The genotyping results confirmed that this marker exhibited DNA polymorphism within the tested population, with clear genotyping, making it suitable for distinguishing different genotypes in wheat germplasm resources. Association analysis revealed that wheat varieties carrying *TaGGR-6A-Hap II* had significantly higher chlorophyll content in their flag leaves than those carrying *TaGGR-6A-Hap I*. The presence of unique transcription factor binding sites, MYB and ARE, in the *TaGGR-6A-Hap II* promoter sequence may be the reason for its advantageous characteristics. Relevant studies have shown that MYB-related transcription factors regulate the expression of genes related to chloroplast biosynthesis by binding to their promoter regions [38]. These genes are involved in various processes such as chlorophyll biosynthesis, CO_2 fixation, photorespiration, and photosystem assembly and repair. *TaGGR-6A-Hap II* positively influenced the chlorophyll content of wheat flag leaves across various environments, thereby enhancing the stabilization and improvement of wheat yield. In order to understand the function of this gene more comprehensively, promoter-reporter gene detection and gene editing using advanced technologies such as CRISPR/Cas9 are planned. This will help to verify the specific effects of these SNPs on gene expression and comprehensively analyze the role of *TaGGR-6A* in wheat physiological processes, providing more precise genetic information and breeding strategies for future wheat breeding.

Conclusion

In this study, we succeed in deciphering key genomic regions and CGs related to photosynthetic efficiency in wheat by integrating MQTL analysis and GWAS. A total

of 74 MQTLs associated with photosynthetic efficiency were identified while more than half of these MQTLs were validated through MTA in 18 GWAS, with 11 being confirmed as core MQTLs. As many as 3,102 CGs were identified within the MQTL regions where 1,043 CGs with more than 2 TPM were highly expressed in leaves, spikes, and stems and 186 CGs involved in the top 20 of KEGG enrichment pathways. Among these, the key CG *TaGGR-6A* related to porphyrin metabolism was selected for the further haplotype analysis. The positive selection for dominant haplotype *TaGGR-6A-Hap II* with high flag leaf chlorophyll content was validated and a functional KASP molecular marker for *TaGGR-6A* was developed that could be directly applied to wheat molecular marker-assisted selection breeding. This work will help to lay a foundation for the great application potential in molecular genetic improvement of photosynthetic efficiency of these key CGs.

Materials and methods

QTL data collection

For QTLs controlling for photosynthetic efficiency traits, a comprehensive screening of studies published between 2007 and 2024 was conducted using the Web of Science (https://www.webofscience.com, Accessed April 2024) and China National Knowledge Infrastructure Network (https://www.cnki.net/, Accessed April 2024). The initia lly screened QTLs are closely related to photosynthetic efficiency. The QTLs related to photosynthetic efficiency mainly include photosynthetic parameters and photosynthetic-related traits. Among them, the parameters of photosynthesis mainly include Pn, Gs, Tr, Ci, SPAD, chlorophyll content (Chl), photosynthetic pigments: Chla, Chla/b, chlorophyll b (Chlb), carotenoids (Car), and chlorophyll fluorescence parameters, including Fm, Fv/Fm, CCI, initial fluorescence (Fo), variable fluorescence (Fv), potential activity index of PSII reaction center (Fv/Fo). The morphological traits of leaves and stomatal-related characteristics that significantly impact photosynthetic efficiency were selected as follows: FLL, FLW, FLA, FLANG, SL, flag leaf perimeter (FLP), flag leaf length/width ratio (FLR), stomatal width (SW), stomatal density (SD), and stomatal area (SA) (Fig. 1c).

For each initial QTL related to photosynthetic efficiency, the following key information was collected: (1) The type and size of the population used for QTL mapping; (2) LOD; (3) PVE or R^2 value of the QTL; (4) Flanking markers or markers closely linked to QTL. QTLs lacking LOD and R^2 values were assumed to be 3 and 10%, respectively [25, 39]. For QTLs with missing CI, the following standard formulas were used to re-estimate the CI for each initial QTL based on different population types and sizes: (1) For F_2 populations, CI = 530 / (N × PVE); (2) For RIL populations, CI = 163 / (N× PVE); (3) For DH populations, CI = 287 / (N× PVE). Here, N represents the size of the mapping population used for QTL analysis, and PVE represents the contribution of the initial QTL to phenotypic variation [40].

Consensus map construction and QTL projection

The high-density reference genetic map obtained from two dense genetic maps contained 14,548 markers including SSR, DArT, SNP and other types of markers [41–43]. The total length of the reference map was 4813.72 cM, with individual chromosome lengths ranging from 155.6 cM to 350.11 cM in the 21 linkage groups. From 66 independent QTL studies, 76 independent genetic maps were extracted originating from 76 mapping populations. BioMercator V4.2.3 [28] is capable of integrating and analyzing QTL data from different studies and mapping populations, identifying consensus QTLs through MQTL analysis methods. The ConsMap program provided by BioMercator v4.2.3 [44] was utilized to project individual maps from each QTL study onto the reference map. The information of the initial QTL, including QTL name, position (on the original genetic map), CI value, R^2, and LOD value were extracted from corresponding studies. Using the QTLProj program in BioMercator v4.2.3, each QTL was mapped from its position on the original genetic map to the corresponding position on the consensus map. QTLs that could not be mapped onto the consensus map were excluded due to the lack of corresponding common markers on the consensus map or because their positions were outside the range of the consensus map. This step effectively eliminates QTL that may introduce errors due to uneven marker density or other inconsistencies, by only including QTL with corresponding common markers on the consensus map.

MQTL analysis

The MQTL analysis was conducted for each chromosome using the integrated consensus map and initial QTLs by BioMercator v4.2.3 software. Based on the number of initial QTLs mapped on each chromosome, two different methods were employed for MQTL analysis: (1) When the number of initial QTLs was less than 10, the method proposed by Goffinet and Gerber was utilized [45]. This method allowed for the derivation of five MQTL models, each with an Akaike Information Criterion (AIC) value of 1, 2, 3, 4, or N. The model with the smallest AIC value was selected to determine the MQTL region. (2) When the number of initial QTLs on a chromosome exceeded 10, the "two-step method" proposed by Veyrieras was used for calculation [44]. In the first step, potential MQTL numbers were estimated based on selection criteria, including AIC (Akaike Information Criterion), corrected AIC (AICc), AIC model 3 (AIC3),

Bayesian Information Criterion (BIC), and Approximate Weight of Evidence (AWE). Subsequently, among the five models, the one that achieved the lowest value in at least three criteria was selected as the best MQTL model. In the second step, based on the best model selected in the first step, the peak position and 95% CI for each MQTL were calculated. Genomic regions containing two or more initial QTLs were defined as MQTLs.

Localization of MQTL on wheat genome and GWAS validation

The markers at both ends of the MQTL CIs were manually identified to retrieve their flanking or primer sequences using resources such as URGI Wheat (http://wheat-urgi.versailles.inra.fr, Accessed May 2024), Grain Genes (https://wheat.pw.usda.gov/GG3/, Accessed May 2024), DArT (https://www.diversityarrays.com, Accessed May 2024), and the official Illumina website (https://www.illumina.com, Accessed May 2024). Subsequently, the integrated JBrowse tool in the Wheat Genome Database (http://wheatomics.sdau.edu.cn, Accessed May 2024) was utilized to pinpoint the precise physical locations of the MQTL flanking markers on the reference genome of Chinese Spring wheat, annotated by IWGSC_v1.0.

The 18 GWAS datasets on photosynthesis efficiency-related traits published between 2014 and 2024 were collected to validate the accuracy of these MQTL regions. These studies were conducted in six countries, with the wheat population varying from 96 to 543. When the position of a MTA overlaps with the position of an MQTL, it is considered that the MQTL and MTA were physically overlapped. The information on the physical positions of MTAs in these studies was sourced from relevant research or databases.

Homology-based CG identification and expression pattern analysis

In this study, the following specific strategies and steps were taken to identify CGs within MQTL regions: (1) A homology analysis strategy between wheat and rice was employed to identify key CGs within each MQTL region. To achieve this, relevant gene information closely related to rice photosynthetic rate was collected from the National Rice Data Center (https://www.ricedata.cn/, Accessed June 2024). Subsequently, the Triticeae-GeneTribe database (http://wheat.cau.edu.cn/TGT/, Accessed June 2024) was used to find the homologous genes in wheat [46]. After screening, these wheat homologous genes located within MQTL intervals were considered important CGs affecting wheat photosynthesis rate [29]. (2) Homology alignment methods were utilized to explore the remaining MQTL CGs, which were then screened and calculated based on the following strict criteria: Firstly, core MQTLs were selected following the selection criteria proposed by Venske et al. (2019) [39]. These core MQTLs needed to meet the following conditions: (a) The initial number of mapped QTLs must be greater than 2; (b) The physical distance of the MQTL should be less than 20 Mb; (c) The genetic distance should be less than 1.0 cM. Next, for MQTLs within the remaining CI, the formula proposed by Saini et al. (2022) was used to accurately calculate the peak physical positions of the MQTLs [47]. Based on this, CGs discovered within a physical interval of less than 2 Mb (i.e., within a range of 1 Mb on either side of the peak) were further identified and considered as CGs closely associated with wheat photosynthetic rate traits. The peak physical position of an MQTL was calculated using the following formula:

$$\begin{gathered} Peak\,position\,(bp) = \\ start\,position\,(bp) + \\ \left\{ \frac{[end\,position\,(bp) - start\,position\,(bp)}{[end\,position\,(bp) - start\,position\,(bp)} \right\} \\ \left(\frac{CI(95\%)}{2} \right) \end{gathered}$$

The detailed information about the CGs within the MQTL regions was identified by utilizing the WheatGmap database (http://www.wheatgmap.org/) [48]. The expression analysis was performed using the Hexaploid Wheat Expression Database from the Wheat Genomics Database (http://wheatomics.sdau.edu.cn, Accessed June 2024) [49]. This expression database stores RNA-Seq data of genes in the Chinese Spring wheat (*Triticum aestivum*) variety at different developmental stages (such as seedling, tillering, jointing, booting, heading, and grain filling) and in different tissues/organs (such as roots, stems, leaves, spikes, and grains) [50]. GO annotation and KEGG pathway analysis were performed using the GENEDENOVO cloud platform (website: https://www.omicshare.com). During the analysis of transcriptional expression levels, CG genes with at least 2 transcripts per million (TPM ≥ 2, based on standards established by Wagner et al., 2013) were selected [51]. Subsequently, TBtools software [52] was used to intuitively display the expression characteristics of these CG genes in the form of heatmaps based on TPM values.

Development of a specific KASP marker for polymorphism identification of key CG

By analyzing key CG sequences through the Wheat Union database (http://wheat.cau.edu.cn/WheatUnion/, Accessed July 2024), SNP loci within coding regions and promoters were identified [53]. A specific SNP (A/G) located at 2,464 bp downstream from the initiation codon of *TaGGR-6A* was converted into a KASP marker

for genotyping. The KASP marker was designed using the WheatOmics 1.0 platform (http://wheatomics.sdau.edu.cn/) (Table S14). Genotypic data were obtained using the variant information query module, with the upstream and downstream extension length set to 2000 bp. Subsequently, the Cis-acting Regulatory Elements Database (https://bioinformatics.psb.ugent.be/webtools/plantcare/html/, Accessed July 2024) was utilized to predict the number and types of cis-regulatory elements within the promoter region of CGs [54].

This study focused on exploring the correlation between important CGs and flag leaf chlorophyll content using 252 wheat germplasm resources located at the Tongwei farm station (105°19′ E, 35°11′ N, altitude 1750 m) and Zhuanglang farm station (105°98′ E, 35°37′ N, altitude 2110 m), Gansu, China, during the period from 2021 to 2022. The two planting sites were denoted as E1 (Tongwei, 2022) and E2 (Zhuanglang, 2022). The field trials were conducted using a randomized block design with three replicates with a row spacing 20 cm and a row length of 1 m, and each row was planted with 60 seeds. At 14- day after flowering, three plants with consistent growth and normal development were selected from each variety. The SPAD-502 chlorophyll meter was used to measure the chlorophyll content of the wheat flag leaves (Table S11).

Abbreviations

AIC	Akaike information criterion
AICc	Corrected Akaike information criterion (AICc)
AIC3	Akaike information criterion 3
AWE	Approximate weight of evidence
BIC	Bayesian information criterion
CGs	Candidate genes
CI	Confidence interval
DArT	Diversity Arrays Technology
DH	Double haploid
GO	Gene ontology
KASP	Kompetitive allele-specific PCR
KEGG	Kyoto Encyclopedia of Genes and Genomes
LOD	Logarithm of odds ratio score
MQTL	Meta-QTL
PCR	Polymerase chain reaction
PVE	Phenotypic variation explained
QTL	Quantitative trait locus
RILs	Recombinant inbred lines
SNP	Single nucleotide polymorphism
TPM	Transcripts per million
GWAS	Genome-wide association study
MTAs	Marker–trait associations
Pn	Net photosynthetic rate
Gs	Stomatal conductance
Tr	Transpiration rate
Ci	Intercellular CO_2 concentration
Chl	Chlorophyll content
SPAD	The evolution of soil plant analysis development
Chla	Chlorophyll a
Chlb	Chlorophyll b
Car	Carotenoids
Chla/b	Chlorophyll a/chlorophyll b
Fo	Initial fluorescence
Fm	Maximum fluorescence
Fv	Variable fluorescence
Fv/Fm	Maximum quantum yield of PSII
Fv/Fo	Maximum primary yield of PSII photochemistry
CCI	Chlorophyll index
FLL	Flag leaf length
FLW	Flag leaf width
FLA	Flag leaf area
FLANG	Flag leaf angle
FLP	Flag leaf perimeter
FLR	Flag leaf length/width ratio
SL	Stomatal length
SW	Stomatal width
SD	Stomatal density
SA	Stomatal area

Supplementary Information

The online version contains supplementary material available at https://doi.org/10.1186/s12864-025-11472-6.

Supplementary Material 1

Supplementary Material 2

Acknowledgements

We thank the scientists for providing a large amount of resequencing data in the WheatUnion website.

Author contributions

MC conducted analysis and wrote the draft of manuscript. TC, LY, ZC, JM, BK, JL, CC, KG, PZ and LG performed data analysis. DY conceived and designed the experiments, reviewed, and edited the writing of the manuscript. All authors read and approved the final manuscript.

Funding

This work was financially supported by the Key Sci & Tech Special Project of Gansu Province (22ZD6NA009), the Breakthrough Project in Seed Industry of Gansu Province (GYGG-2024-2), the Innovative Research Group Project of Gansu Province (24JRRA633), the Major Cultivation Project for University Research and Innovation Platforms of Gansu Province (2024CXPT-01), the Development Fund Project of National Guiding Local Science and Technology (23ZYQA0322), the National Natural Science Foundation of China (32260520, 32360518, 32160487, 32401920), the Industrial Support Plan of Colleges and Universities in Gansu Province (2022CYZC-44).

Data availability

No datasets were generated or analysed during the current study.

Declarations

Ethics approval and consent to participate

Not applicable.

Consent for publication

Not applicable.

Competing interests

The authors declare no competing interests.

Author details

[1]State Key Laboratory of Aridland Crop Science, Gansu Agricultural University, Lanzhou 730070, China
[2]College of Life Science and Technology, Gansu Agricultural University, Lanzhou 730070, China
[3]College of Agronomy, Gansu Agricultural University, Lanzhou 730070, China

Received: 29 December 2024 / Accepted: 11 March 2025
Published online: 22 March 2025

References

1. Liu J, Wang D, Liu M, Jin M, Sun X, Pang Y, et al. QTL mapping for agronomic important traits in well-adapted wheat cultivars. Agronomy. 2024;14:940.
2. Guarin JR, Martre P, Ewert F, Webber H, Dueri S, Calderini D, et al. Evidence for increasing global wheat yield potential. Environ Res Lett. 2022;17:124045.
3. Cai C, Lv L, Wei S, Zhang L, Cao W. How does climate change affect potential yields of four staple grain crops worldwide by 2030? PLoS ONE. 2024;19:e0303857.
4. Shi X, Cui F, Han X, He Y, Zhao L, Zhang N, et al. Comparative genomic and transcriptomic analyses uncover the molecular basis of high nitrogen-use efficiency in the wheat cultivar Kenong 9204. Mol Plant. 2022;15:1440–56.
5. Batista-Silva W, da Fonseca-Pereira P, Martins AO, Zsögön A, Nunes-Nesi A, Araújo WL. Engineering improved photosynthesis in the era of synthetic biology. Plant Commun. 2020;1:100032.
6. Singh J, Pandey P, James D, Chandrasekhar K, Achary VMM, Kaul T, et al. Enhancing C3 photosynthesis: an outlook on feasible interventions for crop improvement. Plant Biotechnol J. 2014;12:1217–30.
7. Głowacka K, Kromdijk J, Salesse-Smith CE, Smith C, Driever SM, Long SP. Is Chloroplast size optimal for photosynthetic efficiency? New Phytol. 2023;239:2197–211.
8. Li R, He Y, Chen J, Zheng S, Zhuang C. Research progress in improving photosynthetic efficiency. Int J Mol Sci. 2023;24:9286.
9. Matthews ML, Burgess SJ. How much could improving photosynthesis increase crop yields? A call for systems-level perspectives to guide engineering strategies. Curr Opin Biotechnol. 2024;88:103144.
10. Yu M, Chen H, Mao S-L, Dong K-M, Hou D-B, Chen G-Y. Contribution of photosynthetic- and yield-related traits towards grain yield in wheat at the individual quantitative trait locus level. Biotechnol Biotechnol Equip. 2020;34:1188–97.
11. Gu Y, Wang Y, Wu Y, Warner TA, Guo T, Ai H, et al. Novel 3D photosynthetic traits derived from the fusion of UAV lidar point cloud and multispectral imagery in wheat. Remote Sens Environ. 2024;311:114244.
12. Chen J, Cao F, Li H, Shan S, Tao Z, Lei T, et al. Genotypic variation in the grain photosynthetic contribution to grain filling in rice. J Plant Physiol. 2020;253:153269.
13. Li Y, Tao F, Hao Y, Tong J, Xiao Y, He Z, et al. Variations in phenological, physiological, plant architectural and yield-related traits, their associations with grain yield and genetic basis. Ann Botany. 2023;131:503–19.
14. Liu C, Sack L, Li Y, Zhang J, Yu K, Zhang Q, et al. Relationships of stomatal morphology to the environment across plant communities. Nat Commun. 2023;14:6629.
15. Du D, Li Z, Yuan J, He F, Li X, Wang N, et al. The TaWAK2-TaNAL1-TaDST pathway regulates leaf width via cytokinin signaling in wheat. Sci Adv. 2024;10:eadp5541.
16. Li N, Dong F, Liu T, Yang J, Shi Y, Wang S, et al. Quantitative trait loci mapping and candidate gene analysis of stoma-related traits in wheat (*Triticum aestivum* L.) glumes. PeerJ. 2022;10:e13262.
17. Niu K-X, Chang C-Y, Zhang M-Q, Guo Y-T, Yan Y, Sun H-J, et al. Suppressing ASPARTIC PROTEASE 1 prolongs photosynthesis and increases wheat grain weight. Nat Plants. 2023;9:965–77.
18. Yan Y, Wang M-L, Guo Y-T, Ding C-H, Niu K-X, Li X-M, et al. HSP90.2 promotes CO assimilation rate, grain weight and yield in wheat. Plant Biotechnol J. 2023;21:1229–39.
19. Ma J, Tu Y, Zhu J, Luo W, Liu H, Li C, et al. Flag leaf size and posture of bread wheat: genetic dissection, QTL validation and their relationships with yield-related traits. Theor Appl Genet. 2020;133:297–315.
20. Zanella CM, Rotondo M, McCormick-Barnes C, Mellers G, Corsi B, Berry S, et al. Longer epidermal cells underlie a quantitative source of variation in wheat flag leaf size. New Phytol. 2023;237:1558–73.
21. Sahranavard N, Jorjani E, Sabouri H, Alegh SM, Katouzi M. Mapping QTLs controlling grain and leaf traits in Iranian wheat Recombinant inbred lines. Plant Mol Biol Rep. 2024;42:394–409.
22. Sahranavard N, Jorjani E, Sabouri H, Alegh SM, Katouzi M. Detecting QTLs controlling chlorophyll fluorescence parameters in Iranian wheat Recombinant inbred lines. Plant Gene. 2024;37:100437.
23. An Q, Li C, Li H, Zheng Q, Li B, Li Z. An analysis of the genetic relation between photosynthesis and yield-related traits in wheat. Agriculture. 2022;12:560.
24. Daware AV, Srivastava R, Singh AK, Parida SK, Tyagi AK. Regional association analysis of MetaQTLs delineates candidate grain size genes in rice. Front Plant Sci. 2017;8.
25. Khahani B, Tavakol E, Shariati V, Fornara F. Genome wide screening and comparative genome analysis for Meta-QTLs, ortho-MQTLs and candidate genes controlling yield and yield-related traits in rice. BMC Genomics. 2020;21:294.
26. Welcker C, Sadok W, Dignat G, Renault M, Salvi S, Charcosset A, et al. A common genetic determinism for sensitivities to soil water deficit and evaporative demand: meta-analysis of quantitative trait loci and introgression lines of maize. Plant Physiol. 2011;157:718–29.
27. Arcade A, Labourdette A, Falque M, Mangin B, Chardon F, Charcosset A, et al. BioMercator: integrating genetic maps and QTL towards discovery of candidate genes. Bioinformatics. 2004;20:2324–6.
28. Sosnowski O, Charcosset A, Joets J. BioMercator V3: an upgrade of genetic map compilation and quantitative trait loci meta-analysis algorithms. Bioinformatics. 2012;28:2082–3.
29. Yang Y, Amo A, Wei D, Chai Y, Zheng J, Qiao P, et al. Large-scale integration of meta-QTL and genome-wide association study discovers the genomic regions and candidate genes for yield and yield-related traits in bread wheat. Theor Appl Genet. 2021;134:3083–109.
30. Sharma D, Kumari A, Sharma P, Singh A, Sharma A, Mir ZA, et al. Meta-QTL analysis in wheat: progress, challenges and opportunities. Theor Appl Genet. 2023;136:247.
31. Du B, Wu J, Islam MS, Sun C, Lu B, Wei P, et al. Genome-wide meta-analysis of QTL for morphological related traits of flag leaf in bread wheat. PLoS ONE. 2022;17:e0276602.
32. Guo K, Chen T, Zhang P, Liu Y, Che Z, Shahinnia F, et al. Meta-QTL analysis and in-silico transcriptome assessment for controlling chlorophyll traits in common wheat. Plant Genome. 2023;16:e20294.
33. Kong B, Ma J, Zhang P, Chen T, Liu Y, Che Z, et al. Deciphering key genomic regions controlling flag leaf size in wheat via integration of meta-QTL and in Silico transcriptome assessment. BMC Genomics. 2023;24:33.
34. Quraishi UM, Pont C, Ain Q, Flores R, Burlot L, Alaux M et al. Combined genomic and genetic data integration of major agronomical traits in bread wheat (*Triticum aestivum* L). Front Plant Sci. 2017;8.
35. Gutbrod K, Romer J, Dörmann P. Phytol metabolism in plants. Prog Lipid Res. 2019;74:1–17.
36. Gan P, Liu F, Li R, Wang S, Luo J. Chloroplasts— beyond energy capture and carbon fixation: tuning of photosynthesis in response to chilling stress. Int J Mol Sci. 2019;20:5046.
37. Li H, Wang Y, Ye M, Li S, Li D, Ren H, et al. Dynamical and allosteric regulation of photoprotection in light harvesting complex II. Sci China Chem. 2020;63:1121–33.
38. Frangedakis E, Yelina NE, Billakurthi K, Hua L, Schreier T, Dickinson PJ, et al. *MYB*-related transcription factors control Chloroplast biogenesis. Cell. 2024;187:4859–e487622.
39. Venske E, dos Santos RS, Farias Dda, Rother R, da Maia V, Pegoraro LC. C, Meta-analysis of the QTLome of fusarium head blight resistance in bread wheat: refining the current puzzle. Front Plant Sci. 2019;10.
40. Darvasi A, Soller M. A simple method to calculate resolving power and confidence interval of QTL map location. Behav Genet. 1997;27:125–32.
41. Maccaferri M, Zhang J, Bulli P, Abate Z, Chao S, Cantu D, et al. A genome-wide association study of resistance to Stripe rust (Puccinia striiformis F. Sp. tritici) in a worldwide collection of hexaploid Sp.ing wheat (Triticum aestivum L). G3 Genes|Genomes|Genetics. 2015;5:449–65.
42. Soriano JM, Alvaro F. Discovering consensus genomic regions in wheat for root-related traits by QTL meta-analysis. Sci Rep. 2019;9:10537.
43. Bilgrami SS, Ramandi HD, Shariati V, Razavi K, Tavakol E, Fakheri BA, et al. Detection of genomic regions associated with tiller number in Iranian bread wheat under different water regimes using genome-wide association study. Sci Rep. 2020;10:14034.
44. Veyrieras J-B, Goffinet B, Charcosset A. MetaQTL: a package of new computational methods for the meta-analysis of QTL mapping experiments. BMC Bioinformatics. 2007;8:49.
45. Goffinet B, Gerber S. Quantitative trait loci: A meta-analysis. Genetics. 2000;155:463–73.
46. Chen Y, Song W, Xie X, Wang Z, Guan P, Peng H, et al. A collinearity-incorporating homology inference strategy for connecting emerging assemblies in the triticeae tribe as a pilot practice in the plant pangenomic era. Mol Plant. 2020;13:1694–708.
47. Saini DK, Srivastava P, Pal N, Gupta PK. Meta-QTLs, ortho-meta-QTLs and candidate genes for grain yield and associated traits in wheat (*Triticum aestivum* L). Theor Appl Genet. 2022;135:1049–81.

48. Zhang L, Dong C, Chen Z, Gui L, Chen C, Li D, et al. WheatGmap: a comprehensive platform for wheat gene mapping and genomic studies. Mol Plant. 2021;14:187–90.
49. Ma S, Wang M, Wu J, Guo W, Chen Y, Li G, et al. WheatOmics: A platform combining multiple omics data to accelerate functional genomics studies in wheat. Mol Plant. 2021;14:1965–8.
50. International Wheat Genome Sequencing Consortium (IWGSC). A chromosome-based draft sequence of the hexaploid bread wheat (Triticum aestivum) genome. Science. 2014;345:1251788.
51. Wagner GP, Kin K, Lynch VJ. A model based criterion for gene expression calls using RNA-seq data. Theory Biosci. 2013;132:159–64.
52. Chen C, Chen H, Zhang Y, Thomas HR, Frank MH, He Y, et al. TBtools: an integrative toolkit developed for interactive analyses of big biological data. Mol Plant. 2020;13:1194–202.
53. Wang W, Wang Z, Li X, Ni Z, Hu Z, Xin M, et al. SnpHub: an easy-to-set-up web server framework for exploring large-scale genomic variation data in the post-genomic era with applications in wheat. GigaScience. 2020;9:giaa060.
54. Lescot M, Déhais P, Thijs G, Marchal K, Moreau Y, Van de Peer Y, et al. PlantCARE, a database of plant cis-acting regulatory elements and a portal to tools for in Silico analysis of promoter sequences. Nucleic Acids Res. 2002;30:325–7.

Publisher's note